RAC1^{P29S} is a spontaneously activating cancer-associated GTPase

Matthew J. Davis[a,b], Byung Hak Ha[a], Edna C. Holman[c], Ruth Halaban[c], Joseph Schlessinger[a,1], and Titus J. Boggon[a,1]

Departments of [a]Pharmacology, [b]Genetics, and [c]Dermatology, Yale University School of Medicine, New Haven, CT 06520

Contributed by Joseph Schlessinger, December 3, 2012 (sent for review November 17, 2012)

RAC1 is a small, Ras-related GTPase that was recently reported to harbor a recurrent UV-induced signature mutation in melanoma, resulting in substitution of P29 to serine (RAC1^{P29S}), ranking this the third most frequently occurring gain-of-function mutation in melanoma. Although the Ras family GTPases are mutated in about 30% of all cancers, mutations in the Rho family GTPases have rarely been observed. In this study, we demonstrate that unlike oncogenic Ras proteins, which are primarily activated by mutations that eliminate GTPase activity, the activated melanoma RAC1^{P29S} protein maintains intrinsic GTP hydrolysis and is spontaneously activated by substantially increased inherent GDP/GTP nucleotide exchange. Determination and comparison of crystal structures for activated RAC1 GTPases suggest that RAC1^{F28L}—a known spontaneously activated RAC1 mutant—and RAC1^{P29S} are self-activated in distinct fashions. Moreover, the mechanism of RAC1^{P29S} and RAC1^{F28L} activation differs from the common oncogenic mutations found in Ras-like GTPases that abrogate GTP hydrolysis. The melanoma RAC1^{P29S} gain-of-function point mutation therefore represents a previously undescribed class of cancer-related GTPase activity.

cancer | cell signaling | x-ray crystallography | cytoskeleton | GEF-independent GTPase exchange

RAC1, the Ras-related small GTPase belonging to the Rho family, functions as a binary molecular switch cycling between an inactive GDP-bound "OFF" state and an active GTP-bound "ON" state (1). Its activity is responsible for the regulation of diverse cellular behaviors including NADPH oxidase activation, formation of cortical actin-containing membrane ruffles and lamellipodia, and induction of gene expression programs (2). Accordingly, these functions are tightly controlled through RAC1 lipidation, subcellular localization, protein expression levels, and Rho GDP-dissociation inhibitor (Rho GDI) interactions. In addition, as a GTPase, RAC1 is turned ON by guanine nucleotide exchange factors (GEFs) and is turned OFF by GTPase activating proteins (GAPs) that facilitate GDP/GTP nucleotide exchange and GTP hydrolysis, respectively. Once this regulation is compromised, RAC1 activity is implicated in various steps of oncogenesis including initiation, progression, invasion, and metastasis (3, 4).

In contrast to Ras, RAC1 has rarely been identified as significantly mutated in cancer. Instead, overexpression of RAC1 has been reported in colorectal, pancreatic, breast, and testicular cancers and in various leukemias (5–7). Additionally, a self-activating splice variant of RAC1, RAC1b, was shown to be overexpressed in breast cancer and lung cancer and is thought to mediate the epithelial–mesenchymal transition in lung epithelial cells (8–10). Furthermore, aberrant activation of upstream regulators of RAC1, particularly in the DBL family of GEFs specific for RAC1 (e.g., TIAM1, PREX1, and ECT2), have been implicated in various cancers (11). Although increased GDP→GTP nucleotide exchange in RAC1 (dependent or independent of GEFs) is important for mediating oncogenic effects, it is interesting that mutations or other aberrations in RAC1 GAPs are not commonly cancer-associated (3, 11).

Recently, a recurrent somatic missense mutation at codon 29 of RAC1 that results in substitution of a proline to a serine residue (RAC1^{P29S}) was discovered in up to 9% of sun-exposed melanomas. This discovery makes RAC1 the third most commonly mutated protooncogene in melanoma after BRAF and NRAS (12–14). Additionally, RAC1^{P29S} is the most common cancer-associated recurrent missense mutation in a Rho family GTPase. The structural location of RAC1 codon 29 is distinct from the "hot spot" gain-of-function mutations found in Ras isoforms at codons 12 or 61 present in ∼30% of all cancers (Fig. 1). Whereas the conserved residues at codons 12 and 61 are responsible for interacting with the β and γ phosphates of GTP, P29 is distal from the phosphates and is part of the Switch I region. Biochemical and cell-based assays demonstrated that RAC1^{P29S} is activated and has increased binding activity toward RAC1 effectors, and expression of mutant protein confers increased cell proliferation, altered cell migration, and stimulates membrane ruffling and MAPK signaling (12). Crystallographic analysis of GTP analog-loaded RAC1^{P29S} also revealed an unusual GTP-bound Switch I conformation for a Rho family GTPase (12). Understanding the gain-of-function mechanism is therefore important for dissecting the functional basis for signal activation and has implications for development of potential therapeutic intervention. Therefore, in the current study we have sought to determine the mechanism by which RAC1^{P29S} is activated. We demonstrate that unlike the common cancer-associated mutations in Ras, RAC1^{P29S} is a fast-cycling GTPase that occurs by a mechanism distinct from the previously described fast-cycling RAC1 mutant, RAC1^{F28L}.

Results

RAC1^{P29S} Displays a Fast-Cycling Phenotype. To investigate the mechanism by which the P29S mutation activates RAC1, we first used an in vitro nucleotide exchange assay to monitor intrinsic activation of recombinant RAC1. It has previously been shown that wild-type RAC1 (RAC1^{WT}) undergoes negligible nucleotide exchange while exposed to physiologic levels of Mg^{2+} in vitro (16): This is because Mg^{2+} is a cofactor for regulating RAC1 and other small GTPase nucleotide exchange kinetics, so Mg^{2+} serves as a "gatekeeper" to RAC1 activation (17, 18). Specifically, Mg^{2+} coordination with RAC1 residues in the Switch I, Switch II, and P loops (T35, D57, and T17, respectively) serve to maintain a GDP-bound inactive state (17). Accordingly, chelation of Mg^{2+} with EDTA can significantly increase GDP→GTP exchange in vitro. We therefore used a fluorescently labeled nonhydrolyzable GTP analog, *N*-methylanthraniloyl (MANT) Guanosine 5′-[γ-thio]triphosphate (mGTPγS), to increase fluorescence (excitation λ = 360 nm, emission λ = 440 nm) upon RAC1 binding to monitor nucleotide exchange for RAC1 preloaded with GDP (RAC1-GDP) under differing levels of Mg^{2+}. In agreement with previous results (16), we found that under physiologic levels of Mg^{2+}, RAC1^{WT} displays marginal mGTPγS loading but demonstrates rapid GDP→mGTPγS exchange when Mg^{2+} is chelated by addition of 20 mM EDTA (Fig. 2*A*). In contrast, RAC1^{P29S} undergoes inherent mGTPγS loading without addition of EDTA (Fig. 2*A*). Quantification of the inherent nucleotide exchange rates (k_{obs}) of RAC1^{WT}

Author contributions: M.J.D., B.H.H., J.S., and T.J.B. designed research; M.J.D. and B.H.H. performed research; E.C.H. and R.H. contributed new reagents/analytic tools; M.J.D., B.H.H., J.S., and T.J.B. analyzed data; and M.J.D., B.H.H., J.S., and T.J.B. wrote the paper.

The authors declare no conflict of interest.

Database deposition: The atomic coordinates and structure factors have been deposited in the Protein Data Bank, www.pdb.org (PDB ID codes 4GZL and 4GZM).

[1]To whom correspondence may be addressed. E-mail: Joseph.Schlessinger@Yale.edu or Titus.Boggon@yale.edu.

This article contains supporting information online at www.pnas.org/lookup/suppl/doi:10.1073/pnas.1220895110/-/DCSupplemental.

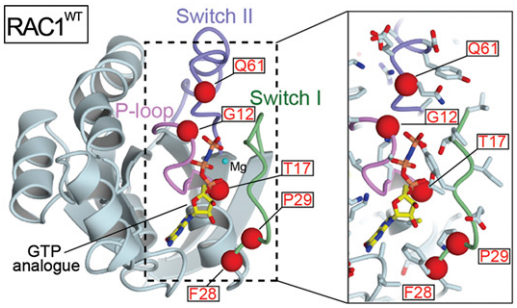

Fig. 1. Structural map of RAC1. Structure of GMP-PNP–loaded RAC1^{WT} (PDB ID code 3TH5) (12) with key regions indicated shown in cartoon format. Red spheres identify the residues described in the paper. The exploded view shows the Switch regions with side chains in cylinder format. Structural figures generated using CCP4MG (15).

and RAC1^{P29S} before Mg^{2+} chelation demonstrates that RAC1^{P29S} displays significantly increased GDP→mGTPγS exchange compared with RAC1^{WT} ($0.0012 \pm 0.00015\ s^{-1}$ and $0.00037 \pm 0.0001\ s^{-1}$, respectively, $P < 0.01$) (Fig. 2*B* and Figs. S1, and S2*A*). As these results suggested a relative spontaneous activation of RAC1^{P29S}, we next investigated the GDP→mGTPγS exchange of a known spontaneously activated RAC1 mutant, F28L (RAC1^{F28L}). Residue F28 is adjacent to P29, is highly conserved in the Ras superfamily, and is known to stabilize the guanine base of GDP and GTP nucleotides (16, 19). Substitution of F28 to leucine in RAC1 results in spontaneous activation and transforms cells while maintaining GTP hydrolysis, results that suggest a "fast-cycling" phenotype (20). In other Rho family GTPases, the F28L mutation was also found to be fast-cycling, to activate Rho family-mediated signaling pathways, and to induce in vitro cell transformation (16, 20). We therefore

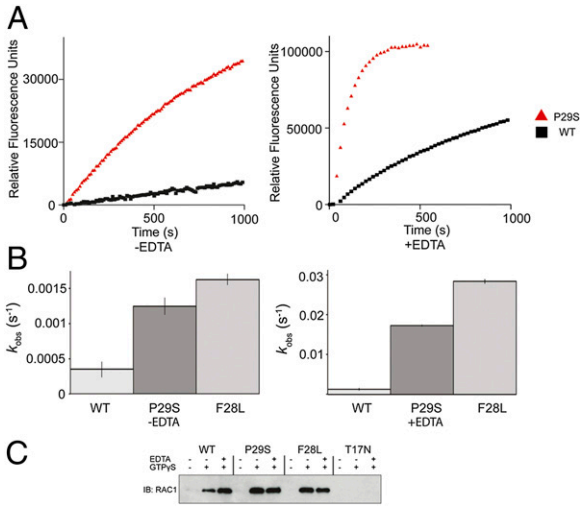

Fig. 2. In vitro nucleotide exchange assays. (*A*) Nucleotide exchange comparison of RAC1^{WT} and RAC1^{P29S}. RAC1^{P29S} is a self-activating mutant as indicated by inherent self-association of mGTPγS without the addition of EDTA (*Left*). EDTA (20 mM) is added to facilitate RAC1^{WT} nucleotide exchange (*Right*). In both experimental conditions, RAC1^{WT} is significantly slower than RAC1^{P29S} ($P < 0.05$). (*B*) Nucleotide exchange rate. Comparison of RAC1^{WT}, RAC1^{P29S}, and RAC1^{F28L} with (*Right*) or without (*Left*) 20 mM EDTA addition. RAC1^{WT} displays marginal exchange without addition of EDTA. SEM for three experiments shown. (*C*) Orthogonal nucleotide exchange pull-down assay. In vitro pull-down of activated GTPγS-loaded RAC1 constructs with the GTPase-binding domain of PAK1. Robust pull-down is observed for RAC1^{P29S} and RAC1^{F28L} with and without 10 mM EDTA. RAC1^{WT} requires 10 mM EDTA to pull-down robustly, and dominant-negative RAC1^{T17N} cannot load GTPγS. Loading controls shown in Fig. S2 *A* and *B*.

compared the nucleotide exchange rate of RAC1^{F28L} to that of RAC1^{P29S}. We found that without addition of EDTA, RAC1^{F28L} spontaneously exchanged GDP for mGTPγS in a similar fashion but displayed a nucleotide exchange rate faster than that of RAC1^{P29S} ($0.0016 \pm 0.00008\ s^{-1}$, $P < 0.05$) (Fig. 2*B* and Fig. S1). On addition of EDTA, both RAC1^{P29S} and RAC1^{F28L} exhibited significantly faster exchange ($0.017 \pm 0.00029\ s^{-1}$ and $0.028 \pm 0.0006\ s^{-1}$, respectively) compared with that after EDTA addition to RAC1^{WT} ($0.0021 \pm 0.00005\ s^{-1}$, $P < 0.001$). RAC1^{F28L} displayed significantly faster exchange than RAC1^{P29S} on addition of EDTA ($P < 0.01$) (Fig. 2*B* and Fig. S1).

The p21-activated kinase (PAK) group of serine-threonine kinases are well-established effectors of RAC1 and other Rho family GTPases (21). We therefore tested whether an in vitro PAK1 pull-down assay could provide further evidence for RAC1^{P29S} as a self-activated GTPase. RAC1^{WT} displayed association with PAK1 when loaded with nonhydrolyzable GTP analog, Guanosine 5′-[γ-thio]triphosphate (GTPγS), but not when preloaded with GDP (Fig. 2*C* and Fig. S2*B*). Furthermore, on addition of GTPγS, both RAC1^{P29S} and RAC1^{F28L} show appreciably increased PAK1 binding compared with that of RAC1^{WT} (Fig. 2*C*). As expected, PAK1 did not associate with RAC1^{T17N}, a known dominant-negative mutation that abrogates nucleotide binding (Fig. 2*C*). The addition of EDTA to facilitate GTPγS loading in RAC1^{WT} is comparable to that observed for RAC1^{P29S} and RAC1^{F28L} in the absence of EDTA. This orthogonal method correlates well with the fluorescence exchange assay (Fig. 2 *A* and *B*) and confirms RAC1^{P29S} as a fast-cycling mutant.

RAC1^{P29S} Maintains Its Ability to Hydrolyze GTP. In the Ras superfamily, most of the common hot-spot oncogenic mutations affect the enzyme's ability to hydrolyze GTP resulting in a constitutively GTP-bound activated GTPase (22). We therefore investigated the intrinsic ability of RAC1^{P29S} to hydrolyze GTP. An α-carbon–radiolabeled GTP ([α-^{32}P]GTP) was used as a tracer, and production of [α-^{32}P]GDP was monitored by separation using TLC. Two separate assays demonstrated that RAC1^{P29S} maintains its inherent GTPase hydrolysis activity (Fig. 3 and Fig. S2*C*). First, RAC1 protein was allowed to hydrolyze [α-^{32}P]GTP in reactions containing differing levels of Mg^{2+}. RAC1^{P29S} displayed an increased GTPase activity in all reaction conditions compared with that of RAC1^{WT} but similar [α-^{32}P]GDP production as that of RAC1^{F28L} (Fig. 3*A*). The known hydrolysis-inactive RAC1^{Q61L} mutant used as a control showed no [α-^{32}P]GDP production. Titration of EDTA into these reactions allowed us to determine that in the presence of 20 mM EDTA, RAC1^{WT} yields approximately similar [α-^{32}P]GDP production as that of RAC1^{P29S} or of RAC1^{F28L} at 10 mM EDTA (Fig. 3*A*). This assay suggested that the increase in [α-^{32}P]GDP production of these mutants is due to increased inherent nucleotide exchange rates resulting in an increased enzyme turnover rate. Second, we used a hydrolysis assay (23) to determine if the first-order hydrolysis rate of GTP-bound RAC1 was affected by the mutations. RAC1 was loaded with [α-^{32}P]GTP in the presence of EDTA. [α-^{32}P]GDP production was monitored after hydrolysis was initiated by addition of Mg^{2+} and further nucleotide exchange prevented using excess nonhydrolyzable GTP analog, GTPγS. [α-^{32}P]GDP production was monitored. RAC1^{WT} and the two fast-cycling mutants displayed similar intrinsic GTP hydrolysis rates, and RAC1^{Q61L} was unable to hydrolyze GTP (Fig. 3*B* and Fig. S3). Our data therefore demonstrate that like RAC1^{F28L}, RAC1^{P29S} is a fast cycler, and it maintains similar intrinsic GTP hydrolysis as that of RAC1^{WT}. To investigate the fast-cycling behavior further, we conducted structural studies.

Structural Basis for a Fast-Cycling RAC1 GTPase. In light of our biochemical analyses, we examined the possibility of whether RAC1^{P29S} and RAC1^{F28L} would have similar structural bases for self-activation. We previously determined the structures of RAC1^{P29S} and RAC1^{WT} in the presence of nonhydrolyzable GTP analogs and observed a significant difference in the conformation of the Switch I loop resulting in RAC1^{P29S} adopting a Ras-like Switch I conformation (12). To investigate whether there was a difference between

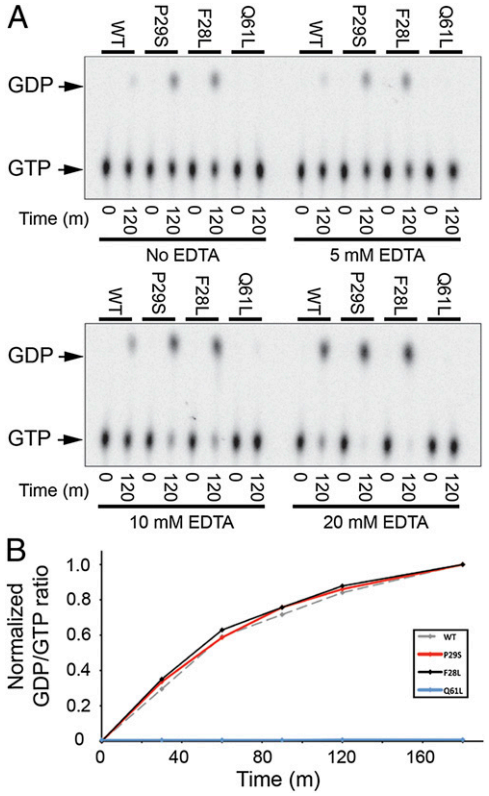

Fig. 3. In vitro GTP hydrolysis assays. (*A*) EDTA tuning of the RAC1 hydrolysis assay. TLC separation of hydrolyzed [α-^{32}P]GTP to [α-^{32}P]GDP is shown for RAC1^{WT}, RAC1^{P29S}, RAC1^{F28L}, and RAC1^{Q61L} under 0, 5, 10, and 20 mM EDTA conditions in a reaction solution containing 10 mM $MgCl_2$. (*B*) Time course of RAC1 first-order GTP hydrolysis assay. Quantification (GDP/GTP ratio) of TLC separation of hydrolyzed [α-^{32}P]GTP to [α-^{32}P]GDP for RAC1^{WT}, RAC1^{P29S}, RAC1^{F28L}, and RAC1^{Q61L} taken at 0, 30, 60, and 120 min. SEM for three experiments <0.1. Fig. S3 contains the SEM errors and reactions for each RAC1 GTPase analyzed.

GTP-loaded RAC1^{F28L} and RAC1^{P29S}, we determined the 2.8 Å crystal structure of RAC1^{F28L} bound to nonhydrolyzable GTP analog GTPγS (Table 1, Fig. 4, and Fig. S4). While the overall structure of RAC1^{F28L} is similar to that of RAC1^{P29S} (rmsd of 0.5 Å over 174 Cα residues), we observe that in contrast to RAC1^{P29S}, RAC1^{F28L} adopts a wild-type–like conformation in its Switch I loop, with increased flexibility (based on temperature factor and electron density analysis) similar to that of solution structures of the CDC42 F28L mutant (24, 25). The F28L mutation in RAC1 also results in a loss of interaction between codon 28 and the nucleoside, suggesting that for RAC1^{F28L}, fast cycling results from reduced affinity for nucleotide. In contrast, for both RAC1^{WT} and RAC1^{P29S}, F28 contacts the guanosine moiety. To confirm the Switch I conformation adopted by catalytically inactive mutants of RAC1, we determined the 2.0 Å crystal structure of RAC1^{Q61L} in complex with nonhydrolyzable GTP analog 5′-Guanylyl imidodiphosphate (GMP-PNP) (Table 1). RAC1^{Q61L} also exhibited a wild-type–like conformation for the Switch I loop (Fig. 4), but like RAC1^{WT} and RAC1^{P29S} also displayed close interactions between F28 and the nucleoside. These structural and biochemical data suggest that RAC1^{F28L} and RAC1^{P29S} are self-activated by different mechanisms, with RAC1^{F28L} self-activation driven by a loss in interaction between the guanine ring and F28, and RAC1^{P29S} is possibly driven by another mechanism, perhaps destabilization of the GDP-loaded inactive state.

Cell Morphological Effects of Distinct Classes of RAC1 Activated Mutants. One of the cellular hallmarks of an activated RAC1 GTPase is the appearance of membrane ruffles (20, 26). We previously demonstrated that transfected GFP-RAC1^{P29S} in cells accumulates in membrane ruffles, which contrasted with a more diffuse cytoplasmic localization for GFP-RAC1^{WT} suggesting that RAC1^{P29S} is activated in vivo. As both RAC1^{F28L} and RAC1^{Q61L} are also activated in vivo, we compared their ability to induce membrane ruffling in live COS-7 cells using N-terminal GFP fusion proteins (20, 26). A ruffling index to score the extent of GFP-RAC1 accumulation at membrane ruffles was used, and an average ruffling index was calculated for each GFP-RAC1 cell population ($n > 20$). RAC1^{WT}-expressing cells displayed an average membrane-ruffling index of 0.54 ± 0.16 ($n = 22$), whereas GFP-RAC1^{P29S}–expressing cells displayed a significantly increased average ruffling index of 1.54 ± 0.14 ($n = 22$, $P < 0.0001$). Both RAC1^{F28L}-expressing cells and RAC1^{Q61L}-expressing cells had similar ruffling indexes (1.54 ± 0.12, $n = 28$, and 1.64 ± 0.14, $n = 22$, respectively) as that of RAC1^{P29S}-expressing cells and were also significantly enriched for membrane ruffles compared with RAC1^{WT}-expressing cells ($P < 0.0001$) suggesting that each class of RAC1 mutation (fast cycling vs. hydrolysis dead) can induce an activated RAC1 cellular phenotype (Fig. 5 *A* and *B*). Notably, GFP-RAC1^{P29S}–expressing cells, RAC1^{F28L}-expressing cells, and RAC1^{Q61L}-expressing cells contained different proportions of multinucleated cells. For RAC1^{P29S}-expressing cells and RAC1^{F28L}-expressing cells, ∼10% of cells harbored two nuclei; in contrast, for RAC1^{Q61L}-expressing cells, ∼45% contained more than one nucleus. Multinucleation has previously been shown for GTPase-defective RAC1 mutants (codon 12 or 61 mutants) and is thought to be because RAC1 activity is a negative regulator of the actomyosin contractile ring construction and can inhibit cytokinesis (27) and RAC1 accumulates in the nucleus during the G2 phase of the cell cycle (28). Finally, we compared the morphological effects of the fast-cycling RAC1 mutants in stable NIH 3T3 fibroblast cell lines. We observed that NIH 3T3 cells expressing the fast-cycling mutants as N-terminal Flag-tagged proteins displayed increased membrane ruffling compared with that of RAC1^{WT} (Fig. 5*B*). We also assayed F-actin stress fibers in conjunction with RAC1 localization and found that both RAC1^{P29S} and RAC1^{F28L} maintained similar F-actin cellular structures (Fig. 5*B*). These assays confirm a similar phenotype for RAC1^{P29S} as that of known RAC1 activating mutations.

Discussion

In this study, we investigate the properties of the mutated Rho family GTPase, RAC1^{P29S}. Discovery of the P29S mutation has placed RAC1 as a commonly mutated gene in melanoma and has highlighted the potential of RAC1 effector pathways as potential therapeutic targets (12, 13). Strikingly, this is the most commonly found recurrent missense mutation to be discovered in a Rho family GTPase. Additionally, the location of P29S is distinct from the commonly found oncogenic mutations in the Ras oncogenes. We therefore studied the biochemical and structural properties of RAC1^{P29S} in comparison with other well-studied RAC1 mutations.

We found that RAC1^{P29S} is a spontaneously activating GTPase with significantly increased inherent GDP→GTP nucleotide exchange compared with that of RAC1^{WT}. This behavior is similar to the previously described RAC1^{F28L} fast-cycling mutant, although notably we found that RAC1^{F28L} displays faster mGTPγS association kinetics than RAC1^{P29S}. We corroborated RAC1^{P29S} as a fast-cycling GTPase by an orthogonal nucleotide exchange assay that tested the ability of GDP-loaded RAC1 to pull-down with the GTPase-binding domain of PAK1. Both assays suggest that RAC1^{P29S} and RAC1^{F28L} are able to exchange GDP for GTP (or GTP analog) without chelation of Mg^{2+}. Additionally, we found that RAC1^{P29S} maintains its inherent ability to hydrolyze GTP. This contrasts with oncogenic forms of Ras that lose their enzymatic activity. We do not know of another frequently recurrent cancer-associated GTPase mutation where spontaneous activation is observed, although P29L in RAC2 has been infrequently observed in melanoma and breast cancer (29, 30), potentially suggesting that fast-cycling mutations in other Rho family GTPases could also be associated with cancer. Notably, cellular imaging of live COS-7 cells suggests that fast-cycling RAC1 mutants (F28L, P29S) behave in a distinct manner in vivo compared with GTPase-defective RAC1 mutants (Q61L), whereas RAC1^{P29S}, RAC1^{F28L},

Table 1. Data collection and refinement statistics

Parameters	$RAC1^{F28L}$ PDB ID code 4GZM	$RAC1^{Q61L}$ PDB ID code 4GZL
Data collection		
Space group	$P2_1$	$P2_12_12_1$
X-ray source and detector	APS 24-ID-C ADSC Q315	NSLS X29 ADSC Q315
Wavelength, Å	0.97922	1.07500
Unit cell: *a*, *b*, *c*; Å	40.1, 98.8, 52.0	49.8, 72.9, 91.6
α, β, γ; °	90, 90.2, 90	90, 90, 90
Resolution range* (Å)	30.0–2.8 (2.91–2.8)	50.0–2.0 (2.07–2.0)
No. of unique reflections	9,692	23,302
Completeness* (%)	99.5 (100)	99.9 (99.8)
R_{sym}* (%)	12.9 (57.8)	11.0 (62.5)
Mean $\langle I\rangle/\langle\sigma I\rangle$*	5.8 (2.4)	14.2 (3.5)
Wilson *B*-factor	99.9	24.0
Redundancy	3.1 (3.7)	6.6 (6.3)
Refinement statistics		
Resolution range* (Å)	50–2.8 (2.87–2.8)	50.0–2.0 (2.05–2.0)
R_{factor}* (%)	25.5 (43.1)	18.6 (25.0)
Free R_{factor}* (%)	28.8 (47.2)	25.0 (32.3)
Free *R* reflections* (%)	4.9 (5.3)	5.2 (5.9)
Free *R* reflections,* no.	485 (38)	1194 (87)
Residues built		
	A/4–177	A/3–30, 32–47, 49–177
	B/4–177	B/2–29, 31–176
No. of water molecules	—	156
Mean *B*-factor (Å^2)		
Protein (chain A/B)	105.7/106.8	36.8/35.9
GTPγS/GMP-PNP (A/B)	113.9/115.1	30.8/28.6
Mg^{2+} (A/B)	74.2/74.4	28.4/29.3
H_2O	—	37.0
Model statistics		
rmsd bond lengths, Å	0.005	0.018
rmsd bond angles, °	0.983	2.024
Ramachandran plot (%) favored/allowed/disallowed	97.7/2.3/0	98.2/1.8/0

ADSC, Area Detector Systems Corporation; APS, Advanced Photon Source; NSLS, National Synchrotron Light Source.
*Indicates high-resolution shell.

and $RAC1^{Q61L}$ all displayed similarly significant induction of membrane ruffling compared with $RAC1^{WT}$. For $RAC1^{Q61L}$, there was a marked increase in cells exhibiting multinucleation (Fig. 5*A*). This could suggest that the GDP/GTP "flux" of Rho family GTPases is important for oncogenesis.

To investigate the mechanism of $RAC1^{P29S}$ activation further, we determined the crystal structures of $RAC1^{F28L}$ and $RAC1^{Q61L}$ and compared these to the structures of $RAC1^{WT}$ and $RAC1^{P29S}$ that we have recently described (12). Although the overall architectures were very similar, the conformation of the Switch I loops of $RAC1^{P29S}$ and $RAC1^{F28L}$ were divergent from each other, with $RAC1^{P29S}$ showing a Ras-like Switch I conformation and $RAC1^{F28L}$ displaying increased flexibility. For $RAC1^{F28L}$, this is probably due to the loss of the phenylalanine benzyl group and consequent reduced stabilizing interactions with nucleotide. On comparison of the GTP analog-loaded crystal structures of $RAC1^{P29S}$ and $RAC1^{F28L}$, it seems clear that the basis for $RAC1^{P29S}$ fast-cycling is not due to reduced interaction with GTP, rather the GDP-loaded state may be destabilized (13). Although destabilization by P29S mutation may preclude cocrystallization of $RAC1^{P29S}$ with GDP, this could be a tractable NMR target.

Mutation of codon 29 could also impact the interactions of RAC1 with GTPase regulatory proteins, Rho GDIs, GAPs, and GEFs, and with downstream effectors. The current studies do not provide a clear understanding of how the interactions of RAC1 with regulators and effectors is affected by P29S or what is the impact of the P29S substitution on binding affinities for GTP or GDP, but our results allow some predictions. Specifically, for GDI interactions, structural analyses of Rho GTPases in complex with Rho GDIs suggest that P29 is distal from the bound GDI by over 12Å, therefore unlikely directly to impact the binding interface. However, these interactions are dependent on the GTP-binding state of the GTPase (31), implying that for the fast-cycling $RAC1^{P29S}$, there could be altered interactions with GDI. For GAP-mediated hydrolysis, although P29 is distal from the site of hydrolysis, it has previously been shown that allosteric effects can impact GAP-

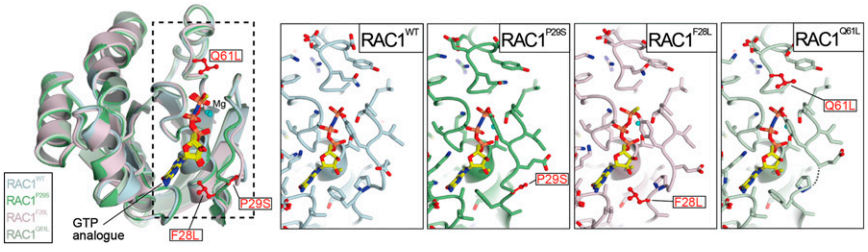

Fig. 4. Comparison of GTP analog-loaded RAC1 crystal structures. Crystal structures of $RAC1^{F28L}$ and $RAC1^{Q61L}$ are compared with $RAC1^{WT}$ (PDB ID code 3TH5) (12) and $RAC1^{P29S}$ (PDB ID code 3SBD) (12). Dashed box indicates region shown in the exploded views. Residues mutated in this study are indicated.

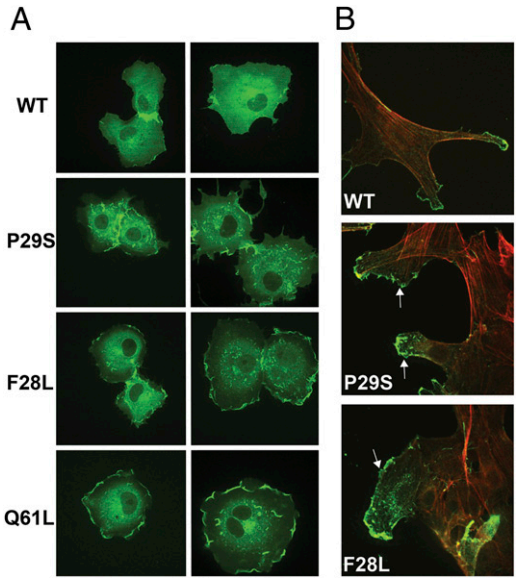

Fig. 5. RAC1^{P29S} exhibits an activated cellular phenotype in live and fixed cells. (*A*) Live COS-7 cells ectopically expressing GFP-RAC1^{WT}, GFP-RAC1^{P29S}, GFP-RAC1^{F28L}, and GFP-RAC1^{Q61L} were imaged using spinning-disk confocal microscopy. Membrane ruffles as indicated by accumulation of GFP-RAC1 signal were observed for GFP-RAC1^{P29S}–, GFP-RAC1^{F28L}–, and GFP-RAC1^{Q61L}–expressing cells. RAC1 ^{WT} exhibited a more diffuse pattern with marginal membrane ruffling at cell edges. (*B*) NIH 3T3 cells stably expressing 3×-Flag-RAC1^{WT}, 3×-Flag-RAC1^{P29S}, and 3×-Flag-RAC1^{F28L} were immunostained with anti-FLAG and probed with Alexa-Fluor 488 to visualize RAC1 expression, and subcellular localization and integrity of F-actin–containing stress-fibers was visualized through staining with rhodamine phalloidin. In both RAC1^{P29S}- and RAC1^{F28L}-expressing cells, membrane ruffling was observed as in COS-7 cells; ruffling is indicated with white arrows.

mediated hydrolysis for Ras and elongation factor Tu (EF-Tu) (32, 33), therefore there is the possibility that allosteric effects could play a role for RAC1^{P29S}. For GEF-mediated nucleotide exchange, although we show that RAC1^{P29S} spontaneously exchanges in the absence of nucleotide exchange factor, the mutation also has the potential to alter response to GEFs. For downstream effectors, there is also the possibility that certain downstream effectors may bind with greater avidity to the RAC1^{P29S} compared with the wild-type protein, potentially affecting discrete signaling pathways. Finally, the impact of P29S mutation on nucleotide-binding affinity could also alter RAC1 signaling. We note that the Rho subfamily of GTPases, which contain an extremely well conserved proline at codon 29, bind GTP in the submicromolar range (18); however, the Ras subfamily of GTPases, which do not have a proline at codon 29, bind GTP in the subnanomolar range (34). We previously showed that RAC1^{P29S} adopts a Ras-like conformation when complexed to a GTP analog (12) (Fig. 4), potentially suggesting altered RAC1^{P29S} affinity for GTP, additional to the driving fast-cycling behavior described here.

The Ras GTPases suffer the most frequent gain-of-function mutations of all oncogenes in cancer (~30%) mainly at codons 12 and 61 (Fig. 1) (35). These oncogenic Ras mutations abrogate GTP hydrolysis (Fig. 3) (36) and mediate their oncogenic potential through the inability of Ras to hydrolyze GTP to GDP, therefore locking the GTPase in an activated state with consequent effector activation (36). Strikingly, until now there have been very rare recurrent cancer-associated mutations discovered in Rho family GTPases, and although mutation of F28 in CDC42 can transform cells (16, 20), it has not yet been found in patients. Furthermore, P29S in RAC1 is the first example of a fast-cycling cancer-associated GTPase mutation that is frequently recurrent in melanoma. Therefore, RAC1^{P29S} represents a previously undescribed class of cancer-associated mutation; a recurrent Rho family spontaneously activated GTPase.

Materials and Methods

In Vitro RAC1 Fluorescent GTPγS Exchange Assay. Purified RAC1 recombinant protein (250 nM) preloaded with GDP. RAC1-GDP was added into loading buffer (20 mM Tris·HCl, pH 7.5/50 mM NaCl/10 mM $MgCl_2$) containing 500 nM mGTPγS with and without 20 mM EDTA (concentration as indicated in Fig. S2 *A* and *B*) with constant stirring at a total volume of 2 mL. The mGTPγS fluorescence was monitored in real time (excitation $\lambda = 360$ nm, emission $\lambda = 440$ nm) using a Photon Technology International SC-500 spectrometer. Rate constants were calculated using GraphPad's single-phase exponential equation ($Y = Y_{max} \times [1 - e^{-kx}]$) to fit the association of mGTPγS proteins as measured through relative fluorescence unit (RFU) increase. Loading controls for these experiments are shown in Fig. S2.

In Vitro RAC1 GTP Hydrolysis Assay. Two in vitro RAC1 GTP hydrolysis assays using a radiolabeled α-carbon GTP ([α-^{32}P]GTP) as a tracer allowed for quantification of produced [α-^{32}P]GDP from remaining [α-^{32}P]GTP using polyethyleneimine (PEI) cellulose TLC plates and a solution phase of 1 M formic acid and 1 M $LiCl_2$. The first assay monitored [α-^{32}P]GDP/[α-^{32}P]GTP + [α-^{32}P]GDP after incubating 1 μM RAC1-GDP in a reaction buffer containing 50 mM Tris·HCl (pH 7.5), 10 mM $MgCl_2$, 10 μg/mL enzyme-grade BSA, 10 μM cold GTP, and 1 μCi/mL [α-^{32}P]GTP (3,000 Ci/mmol) containing various concentrations of EDTA (as indicated in Fig. 3*A*) for 2 h at 20 °C. The second assay monitored [α-^{32}P]GDP/[α-^{32}P]GTP + [α-^{32}P]GDP after first incubating 1 μM RAC1-GDP in a loading buffer containing 50 mM Tris·HCl (pH 7.5), 10 μg/mL enzyme-grade BSA, 10 mM EDTA, 1 μM cold GTP, and 1 μCi/mL [α-^{32}P]GTP (3,000 Ci/mmol) on ice for 30 min. After loading [α-^{32}P]GTP, hydrolysis was initiated with excess $MgCl_2$ (30 mM final concentration), and enzyme turnover was inhibited with excess GTPγS (20 μM final concentration). For both assays at indicated time points, 1 μL of the reaction mixture was stopped in 4 μL of a stop mixture containing 2 mM EDTA and 0.5% SDS, and 1 μL of this reaction stop mixture was spotted on the TLC plate. After the liquid-phase run, the plates were dried and allowed to develop on a Phosphor screen for at least 16 h and imaged. Loading controls for these assays are included in Fig. S2*C*.

In Vitro RAC1 Activation Assay. Purified recombinant RAC1 proteins (30 μM) that had been previously loaded with GDP were either incubated with 500 μM GTPγS with or without 10 mM EDTA to facilitate nucleotide exchange or left bound to GDP at room temperature for 1 h, and exchange was quenched by addition of 10 mM $MgCl_2$ (final volume). Next, 5 μg RAC1 nucleotide complexes was incubated with 5 μg Glutathione Sepharose-bound GST-PAK1-GBD domain (PAK1 amino acids 67–150) and incubated while rotating at 4 °C for 60 min in 500 μL cold pull-down buffer [25 mM Tris·HCl, pH 8.0/40 mM NaCl/30 mM $MgCl_2$/1 mM DTT/1% (vol/vol) Nonidet P-40]. After incubation, beads were washed three times with ice-cold pull-down buffer. Pull-down efficiency was then assayed via immunoblotting. Loading controls of this assay are included in Fig. S2*B*.

Generation of Stable NIH 3T3 Cell Lines. A modified 3× FLAG lacking any enterokinase cleavage site (DYKDHDGDYKDHDIDYKDHDG) was used to N-tag RAC1. NIH 3T3 cells stably expressing these 3×-FLAG-RAC1 constructs were created by transfecting 7.5 μg 3×-FLAG-RAC1 pSMPUW-Hygro (Cell Biolabs) plasmids using Lipofectamine 2000 according to the manufacturer's instructions (Invitrogen) and selected with 200 μg/mL hygromycin for 2 wk. All RAC1 mutants were generated according to the QuikChange site-directed mutagenesis method following the manufacturer's protocol (Agilent Technologies).

Fluorescence Microscopy. COS-7 cells were transiently transfected with 1.5 μg pcDNA3-e*GFP*-RAC1^{WT}, RAC1^{P29S}, RAC1^{F28L}, and RAC1^{Q61L} constructs using Lipofectamine 2000 (Invitrogen) according to the manufacturer's instructions. After transfection, cells were plated on glass-bottom imaging plates (35 mM MatTek No. 1.0) and allowed to recover in DMEM supplemented with 10% (vol/vol) FBS and 1% (vol/vol) penicillin and streptomycin for 24 h. Live COS-7 cells were then imaged using a multicolor spinning-disk confocal UltraVIEW VoX system (PerkinElmer) based on an inverted Olympus microscope equipped with a 1 Kb × 1 Kb electromagnetic charge-coupled device camera (Hamamatsu Photonics) using a 60×, 1.4 N.A. oil objective lens. The system was controlled by Velocity software. For NIH 3T3 stable cell lines, the cells were plated on coverslips and fixed with paraformaldehyde (3.2% vol/vol) and washed again and stained with rhodamine phalloidin for F-actin and immunostained with anti-FLAG antibody with subsequent secondary probing with Alexa-Fluor 488 for RAC1 localization. The same microscopy parameters were used for analysis of stable cell lines. Membrane ruffling was quantified by adapting a previously used method (37). For each cell

examined ($n > 20$ for each construct), a membrane-ruffling index was assigned where 0 = no membrane ruffling, 1 = <25% membrane ruffling present on the cell surface in one defined area, and 2 = two or more discrete areas displaying membrane ruffling present. From the sum of the membrane-ruffling index, an average ruffling index was calculated for each construct. Multinucleated cells were counted manually.

RAC1 Purification for in Vitro Experiments. For in vitro experiments, recombinant $RAC1^{WT}$, $RAC1^{P29S}$, $RAC1^{F28L}$, and $RAC1^{Q61L}$ were expressed as N-terminal hexahistidine (6xHis)-tag in BL21(DE3) cells and induced with 1 mM isopropyl β-D-1-thiogalactopyranoside (IPTG) for 12 h at 16 °C. The fusion protein was affinity purified, and the protein was then loaded on a Superdex 200 HiLoad 26/60 (GE Healthcare) column in a buffer of 20 mM Tris·HCl (pH 8.0), 150 mM NaCl, and 1 mM DTT.

$RAC1^{F28L}$ and $RAC1^{Q61L}$ Expression and Purification for Crystallization. $RAC1^{F28L}$ and $RAC1^{Q61L}$ spanning residues 2–177 were subcloned into a modified pET-28 vector with a 6xHis-tag and cleaved by Tobacco Etch Virus (TEV) protease, which produces N-terminally 6xHis-tagged RAC1. Recombinant $RAC1^{F28L}$ and $RAC1^{Q61L}$ were expressed as N-terminal 6xHis-tagged proteins in BL21-CodonPlus(DE3)RILP cells and induced with 1 mM IPTG for 24 h at 18 °C. Briefly, the recombinant proteins were affinity purified by HisTrap chelating column (GE Healthcare) and then loaded on a Superdex 75 10/300 GL (GE Healthcare) column in a buffer of 20 mM Tris·HCl (pH 8.0), 150 mM NaCl, and 1 mM DTT. For crystallization, the purified proteins were concentrated to 4 mg/mL in a buffer of 20 mM Tris, 150 mM NaCl, 1 mM DTT, 5 mM $MgCl_2$, with 1 mM GTPγS for $RAC1^{F28L}$ or 1 mM GMP-PNP for $RAC1^{Q61L}$.

$RAC1^{F28L}$ and $RAC1^{Q61L}$ Crystallization. Crystals of $RAC1^{F28L}$ were grown by hanging drop methodology in a 1:1 volume ratio of purified $RAC1^{F28L}$ and reservoir solution containing 0.1 M Hepes (pH 7.5), 16–18% (vol/vol) PEG 4000, and 8% (vol/vol) isopropanol at room temperature. Crystals were equilibrated in a cryoprotectant buffer containing reservoir buffer plus 25% (vol/vol) glycerol and were flash frozen in a nitrogen stream at 100 K. X-ray data from a single crystal were collected to 2.8 Å resolution using Beamline 24-ID-C at the Advanced Photon Source (APS). Crystals of $RAC1^{Q61L}$ were grown by hanging drop methodology in a 1:1 volume ratio of purified $RAC1^{Q61L}$ and reservoir solution containing 0.1 M Hepes (pH 7.5), 16–18% (vol/vol) PEG 4000, and 6% (vol/vol) isopropanol at room temperature. Crystals were equilibrated in a cryoprotectant buffer containing reservoir buffer plus 25% (vol/vol) glycerol and were flash frozen in a nitrogen stream at 100 K. X-ray data from a single crystal were collected to 2.0 Å resolution using Beamline X29 at the National Synchrotron Light Source (NSLS).

Structure Determination and Refinement. $RAC1^{F28L}$ and $RAC1^{Q61L}$ data were processed using the HKL2000 package (38), and initial phases were calculated by molecular replacement using the program Phaser (39) with wild-type RAC1 [Protein Data Bank (PDB) ID code 3TH5] (12) used as a search model. Refinements were conducted using REFMAC5 (40) with a maximum-likelihood target and medium non-crystallographic symmetry restraints. The $RAC1^{Q61L}$ data had two translation libration screw groups per molecule (3–77 and 78–177 residues). COOT model-building tools (41) were used for manual model building. Model validation was conducted using MolProbity (42). The final refined models of $RAC1^{F28L}$ and $RAC1^{Q61L}$ have R/R_{free} values of 25.5%/28.8% and 18.6%/25.0%, respectively (Table 1). One hundred percent of residues fall within favored or allowed regions of the Ramachandran plot. Good electron density is observed throughout the structure, including GTPγS and GMP-PNP, however residues G30 (chain A) and E31 and G48 (chain B) in $RAC1^{Q61L}$ are not visible in the electron density. Structures have been deposited in the PDB (PDB ID codes 4GZL and 4GZM).

ACKNOWLEDGMENTS. We thank the NSLS (Beamlines X6A and X29) and APS (Northeastern Collaborative Access Team). This work was supported by National Institutes of Health Grant GM102262 (to T.J.B.), Yale Specialized Programs of Research Excellence (SPORE) in Skin Cancer Grant CA121974 (to R.H.), and Gilead Sciences Grant YG-001-11 (to T.J.B. and J.S.).

1. Vetter IR, Wittinghofer A (2001) The guanine nucleotide-binding switch in three dimensions. *Science* 294(5545):1299–1304.
2. Jaffe AB, Hall A (2005) Rho GTPases: Biochemistry and biology. *Annu Rev Cell Dev Biol* 21:247–269.
3. Vega FM, Ridley AJ (2008) Rho GTPases in cancer cell biology. *FEBS Lett* 582(14):2093–2101.
4. Ellenbroek SI, Collard JG (2007) Rho GTPases: Functions and association with cancer. *Clin Exp Metastasis* 24(8):657–672.
5. Fritz G, Just I, Kaina B (1999) Rho GTPases are over-expressed in human tumors. *Int J Cancer* 81(5):682–687.
6. Schnelzer A, et al. (2000) Rac1 in human breast cancer: Overexpression, mutation analysis, and characterization of a new isoform, Rac1b. *Oncogene* 19(26):3013–3020.
7. Wang J, et al. (2009) Overexpression of Rac1 in leukemia patients and its role in leukemia cell migration and growth. *Biochem Biophys Res Commun* 386(4):769–774.
8. Jordan P, Brazão R, Boavida MG, Gespach C, Chastre E (1999) Cloning of a novel human Rac1b splice variant with increased expression in colorectal tumors. *Oncogene* 18(48):6835–6839.
9. Stallings-Mann ML, et al. (2012) Matrix metalloproteinase induction of Rac1b, a key effector of lung cancer progression. *Sci Transl Med* 4(142):142ra195.
10. Fiegen D, et al. (2004) Alternative splicing of Rac1 generates Rac1b, a self-activating GTPase. *J Biol Chem* 279(6):4743–4749.
11. Wertheimer E, et al. (2012) Rac signaling in breast cancer: A tale of GEFs and GAPs. *Cell Signal* 24(2):353–362.
12. Krauthammer M, et al. (2012) Exome sequencing identifies recurrent somatic RAC1 mutations in melanoma. *Nat Genet* 44(9):1006–1014.
13. Hodis E, et al. (2012) A landscape of driver mutations in melanoma. *Cell* 150(2):251–263.
14. Machesky LM, Sansom OJ (2012) Rac1 in the driver's seat for melanoma. *Pigment Cell Melanoma Res* 25(6):762–764.
15. McNicholas S, Potterton E, Wilson KS, Noble ME (2011) Presenting your structures: The CCP4mg molecular-graphics software. *Acta Crystallogr D Biol Crystallogr* 67(Pt 4):386–394.
16. Lin R, Bagrodia S, Cerione R, Manor D (1997) A novel Cdc42Hs mutant induces cellular transformation. *Curr Biol* 7(10):794–797.
17. Hall A, Self AJ (1986) The effect of Mg^{2+} on the guanine nucleotide exchange rate of p21N-ras. *J Biol Chem* 261(24):10963–10965.
18. Zhang B, Zhang Y, Wang Z, Zheng Y (2000) The role of Mg^{2+} cofactor in the guanine nucleotide exchange and GTP hydrolysis reactions of Rho family GTP-binding proteins. *J Biol Chem* 275(33):25299–25307.
19. Reinstein J, Schlichting I, Frech M, Goody RS, Wittinghofer A (1991) p21 with a phenylalanine 28——leucine mutation reacts normally with the GTPase activating protein GAP but nevertheless has transforming properties. *J Biol Chem* 266(26):17700–17706.
20. Lin R, Cerione RA, Manor D (1999) Specific contributions of the small GTPases Rho, Rac, and Cdc42 to Dbl transformation. *J Biol Chem* 274(33):23633–23641.
21. Dummler B, Ohshiro K, Kumar R, Field J (2009) Pak protein kinases and their role in cancer. *Cancer Metastasis Rev* 28(1-2):51–63.
22. Downward J (2003) Targeting RAS signalling pathways in cancer therapy. *Nat Rev Cancer* 3(1):11–22.
23. Kleuss C, Raw AS, Lee E, Sprang SR, Gilman AG (1994) Mechanism of GTP hydrolysis by G-protein alpha subunits. *Proc Natl Acad Sci USA* 91(21):9828–9831.
24. Adams PD, Oswald RE (2006) Solution structure of an oncogenic mutant of Cdc42Hs. *Biochemistry* 45(8):2577–2583.
25. Adams PD, Loh AP, Oswald RE (2004) Backbone dynamics of an oncogenic mutant of Cdc42Hs shows increased flexibility at the nucleotide-binding site. *Biochemistry* 43(31):9968–9977.
26. Ridley AJ, Paterson HF, Johnston CL, Diekmann D, Hall A (1992) The small GTP-binding protein rac regulates growth factor-induced membrane ruffling. *Cell* 70(3):401–410.
27. Jordan SN, Canman JC (2012) Rho GTPases in animal cell cytokinesis: an occupation by the one percent. *Cytoskeleton (Hoboken)* 69(11):919–930.
28. Michaelson D, et al. (2008) Rac1 accumulates in the nucleus during the G2 phase of the cell cycle and promotes cell division. *J Cell Biol* 181(3):485–496.
29. Berger MF, et al. (2012) Melanoma genome sequencing reveals frequent PREX2 mutations. *Nature* 485(7399):502–506.
30. Sjöblom T, et al. (2006) The consensus coding sequences of human breast and colorectal cancers. *Science* 314(5797):268–274.
31. Michaelson D, et al. (2001) Differential localization of Rho GTPases in live cells: regulation by hypervariable regions and RhoGDI binding. *J Cell Biol* 152(1):111–126.
32. Adamczyk AJ, Warshel A (2011) Converting structural information into an allosteric-energy-based picture for elongation factor Tu activation by the ribosome. *Proc Natl Acad Sci USA* 108(24):9827–9832.
33. Shurki A, Warshel A (2004) Why does the Ras switch "break" by oncogenic mutations? *Proteins* 55(1):1–10.
34. John J, et al. (1993) Kinetic and structural analysis of the Mg(2+)-binding site of the guanine nucleotide-binding protein p21H-ras. *J Biol Chem* 268(2):923–929.
35. Roberts PJ, Der CJ (2007) Targeting the Raf-MEK-ERK mitogen-activated protein kinase cascade for the treatment of cancer. *Oncogene* 26(22):3291–3310.
36. Pylayeva-Gupta Y, Grabocka E, Bar-Sagi D (2011) RAS oncogenes: weaving a tumorigenic web. *Nat Rev Cancer* 11(11):761–774.
37. Cox D, et al. (1997) Requirements for both Rac1 and Cdc42 in membrane ruffling and phagocytosis in leukocytes. *J Exp Med* 186(9):1487–1494.
38. Otwinowski Z, Minor W (1997) Processing of X-ray Diffraction Data Collected in Oscillation Mode. *Methods in Enzymology Volume 276: Macromolecular Crystallography*, eds Carter CW, Jr., and Sweet RM (Academic, New York), Part A, pp 307–326.
39. McCoy AJ, Grosse-Kunstleve RW, Storoni LC, Read RJ (2005) Likelihood-enhanced fast translation functions. *Acta Crystallogr D Biol Crystallogr* 61(Pt 4):458–464.
40. Murshudov GN, Vagin AA, Dodson EJ (1997) Refinement of macromolecular structures by the maximum-likelihood method. *Acta Crystallogr D Biol Crystallogr* 53(Pt 3):240–255.
41. Emsley P, Cowtan K (2004) Coot: Model-building tools for molecular graphics. *Acta Crystallogr D Biol Crystallogr* 60(Pt 12 Pt 1):2126–2132.
42. Davis IW, Murray LW, Richardson JS, Richardson DC (2004) MOLPROBITY: Structure validation and all-atom contact analysis for nucleic acids and their complexes. *Nucleic Acids Res* 32(Web Server issue):W615–W619.